

Embedding Anatomical Characteristics in 3D Models of Lower-limb Sockets through Statistical Shape Modelling

Ana Costa¹, Daniel Rodrigues², Marina Castro², Sofia Assis² and Hélder P. Oliveira^{3,4} ^a

¹Faculty of Engineering of the University of Porto, Portugal

²Adapttech, Porto, Portugal

³INESC-TEC, Porto, Portugal

⁴Faculty of Sciences of the University of Porto, Portugal

Keywords: Principal Component Analysis, Point Cloud Registration, Statistical Shape Models, Lower Limb Sockets, 3D Scanning.

Abstract: Lower limb amputation is a condition affecting millions of people worldwide. Patients are often prescribed with lower limb prostheses to aid their mobility, but these prostheses require frequent adjustments through an iterative and manual process, which heavily depends on patient feedback and on the prosthetist's experience. New computer-aided design and manufacturing technologies have been emerging as a way to improve the fitting process by creating virtual socket models. Statistical Shape modelling was used to create 3D models of transtibial (TT) and transfemoral (TF) sockets. Their generalization errors were, respectively, 6.8 ± 1.8 mm and 10.5 ± 1.6 mm, while specificity errors were 9.7 ± 0.6 mm and 9.8 ± 0.2 mm. In both models, a visual analysis showed that biomechanically meaningful features were captured: the largest variations found for both types were in the length of the residual limb and in the perimeter variation along the limb. The results obtained proved that statistical shape modelling methods can be applied to TF and TT sockets, with several potential applications in the orthoprosthesis field: generation of new plausible shapes and on-demand socket design adjustments.

1 INTRODUCTION

Lower limb loss has been defined as a complete loss, in the transverse anatomical plane, of any part of the lower limb, for any reason. The incidence of limb loss is expected to increase in the coming years, reaching 3.6M in the United States in 2050 (Varma et al., 2014). The two most common levels of amputation are transtibial (below the knee) and transfemoral (above the knee).

Amputation can have a devastating effect on both physical and mental health, with mobility being the main aspect of an amputee's satisfaction with life (Wurdeman et al., 2018). To improve mobility, patients are prescribed with prostheses. Adjusting a prosthesis to a patient is a difficult process, with the most prolonged, iterative part being the fitting of the socket to the residual limb. This process heavily depends, not only on the skill and experience of the prosthetist, but also on patient feedback, which can

sometimes be unreliable, with no quantitative information involved (Paternò et al., 2018).

There have been several attempts, both in industry and academia, to improve this process by applying digital technologies to both the manufacturing and the design of the socket. Computer-Aided Design and Manufacturing (CAD/CAM) systems allow for digitalization of sockets, creating a virtual representation that can be corrected with more accuracy and precision through digital tools (Mehmood et al., 2019). In comparison with the traditional process, this is a faster and cheaper method of socket adjustment. Most importantly, this method provides a significant improvement in the quality of life of amputees compared to traditional fitting techniques (Karakoç et al., 2017).

TF and TT sockets are usually based on a small set of base designs. This implies that shape variability is limited and there are restrictions on what can be considered a valid shape. However, 3D scanners used in the prosthetic field nowadays are blind to this prior knowledge, which could improve the quality of their 3D representations. From this observation,

^a  <https://orcid.org/0000-0002-6193-8540>

our work hypothesizes that, with a diverse enough dataset, a generic model capturing the variability between shapes can be built. From this model, it would then be possible to fit new examples to the universe of possible shapes, thus detecting and eliminating unrealistic scanning artifacts. Such a model would also allow generation of new plausible shapes, which could bypass the need for an initial plaster mold of the residual limb, as well as open up new pathways for the application of machine and deep learning algorithms to this field by using data augmentation. In this work, we validate these hypotheses by using statistical shape modelling techniques with a dataset of 3D scans of lower limb sockets and exploring its applications in the generation of new shapes.

2 RELATED WORK

Statistical Shape Models (SSMs) are based on the assumption that each shape is a deformed version of a reference shape. Therefore, they can be used to analyze differences in a dataset and also to synthesize new, similar shapes (Lindner, 2017).

One of the best known SSMs is the Active Shape Model, which uses landmarks to examine and measure shape change (Cootes et al., 1992). This and similar models, where shapes are represented by a set of corresponding points, are referred to as Point Distribution Models (Huang et al., 2013). The main steps in building a statistical shape model, once a dataset is acquired, are: shape representation, shape registration, model training and evaluation.

Registration can be defined as the process of bringing two or more shapes of the same object or of similar objects into the same reference system (Castellani and Bartoli, 2014). The problem of registering a set of shapes can be tackled in a single-stage fashion or, alternatively, as a two-stage process, where a point-to-point correspondence is established and, independently, an optimal alignment is found. There are several ways to establish correspondence between 3D shapes by applying rigid or non-rigid transformations. In SSMs, automatic registration typically falls into one of the following types: parametrization, distance-based, feature-based or image-based. These methods often solve the alignment and correspondence issue together. When dealing, in particular, with point clouds, a number of local feature descriptors have been proposed, such as point signatures, point feature histograms, signature of histograms of orientations and rotational projection statistics (Yang et al., 2016).

Most often, model building uses Principal Component Analysis (PCA), an algorithm which finds the directions with greatest variance in the training data. SSMs can have many different applications. Modelling human expression and pose is one of the main areas of interest due to their large potential for human-machine interactions (Yang et al., 2011). The other large field of application is medical image segmentation, for detecting abnormalities in anatomical shapes (Cha et al., 2018).

To the authors' best knowledge, relatively little work done has been done with statistical shape analysis in prostheses. Even though the SSM is not the paper's main focus, (Steer et al., 2020) work on methods for socket design based on SSM and finite element analysis stands out the most. A statistical shape model is used to introduce representative morphological variation into a finite element model (which is the paper's main focus). This model is constructed from aligned surface scans of TT plaster casts to which PCA was applied. The principal modes of variation found were the residuum length, related to the amputation height, and the profile, related to how conical or bulbous the limb is.

3 METHODS

This work entailed the collection of a dataset of point clouds of lower limb sockets, described in this section. The point clouds were registered using heuristic techniques for both alignment and point-to-point correspondence. The statistical shape models were built using PCA. All implementations were written in Python 3.7, using NumPy 1.18 (Van Der Walt et al., 2011), scikit-learn 0.23 (Pedregosa et al., 2011) and Open3D 0.9.0 (Zhou et al., 2018).

3.1 Dataset Collection and Characterization

Table 1: Summary of dataset characteristics. Dimensions are in millimeters.

		Height		Perimeter		
		<i>MinH</i>	<i>MaxH</i>	<i>BP</i>	<i>MP</i>	<i>HP</i>
TT	<i>Min</i>	113	166	121	210	230
	<i>Median</i>	175	250	180	300	325
	<i>Max</i>	256	349	256	427	462
TF	<i>Min</i>	138	264	121	252	391
	<i>Median</i>	225	325	220	400	480
	<i>Max</i>	292	426	308	537	650

The point clouds of lower limb sockets were obtained using a 3D stereoscopy and laser-based scanner which

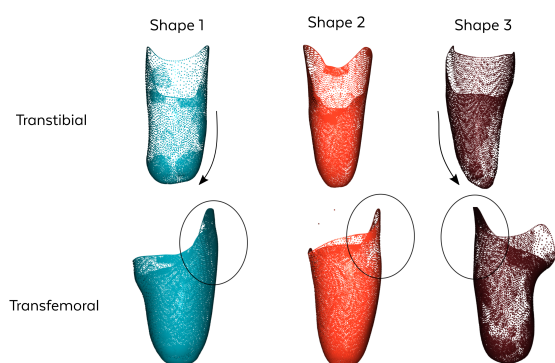


Figure 1: Transtibial and transfemoral sockets from the dataset, in posterior views, with medial leaning and lateral support highlighted.

digitizes the interior surface of sockets¹. These scans were acquired in clinical settings with the use of the data for research purposes authorized. Scans have no associated patient information other than the type of amputation and the leg. For each scan, multiple measures were taken to characterize the socket, namely its full height ($MaxH$) and the maximum height at which the perimeter still corresponds to a full circle ($MinH$), and the socket perimeters at $MinH$, at mid-height and at the bottom (HP , MP and BP , respectively).

Some examples of the dataset can be seen in Figure 1. Anatomical variations such as length of the residual limb or musculature (reflected in a more conical shape) can be seen, along with more distinctive features such as the medial leaning of TT sockets. A total of 30 TT and 21 TF examples were collected. The analysis of their characteristics is summarized in Table 1.

3.2 Point Cloud Registration

3.2.1 Alignment

Due to the inherent differences between shapes of TT and TF sockets, two separate but analogous procedures were followed for registration. For both types of sockets, the final registration result was determined to be a point cloud with as many points as the smallest point cloud in the dataset (4,731 for TT and 11,487 for TF). The acquisition system guarantees that the acquired shapes are all under the same metric referential and that the vertical axes of the sockets are aligned. Therefore, the alignment problem is simplified to a two-dimensional rotation and a translation.

The translation problem was solved by overlapping the centroids of each socket with the origin of the coordinate system.

¹INSIGHT™ Scanner: <https://www.adapttech.eu/insight#knowinsight>

The rotation required an additional pre-processing step: the mirroring of shapes pertaining to the left leg along a radial plane, to harmonize differences between left and right leg. Then, to find the optimal 2D rotation matrix to align the shapes, a landmark present across all shapes (based on domain knowledge) was chosen. The optimal rotation was finally defined as that which brings these landmarks into overlapping positions. For TT sockets, the landmark chosen was the center of the posterior proximal support, as seen in Figure 2a. For TF sockets, the landmark was the center of the medial proximal border, as seen on Figure 2b.

A semi-automatic method was employed to detect these landmarks using the measurements taken for each instance of the dataset.

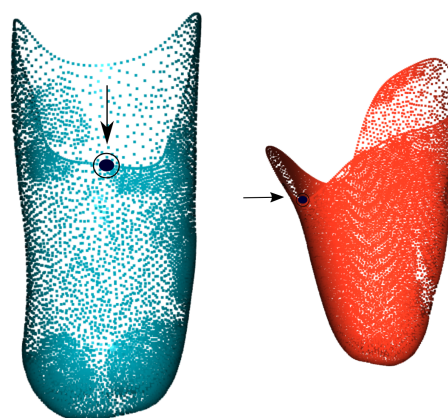
To overlap the landmarks, a socket from the dataset was randomly chosen as the target and all other point clouds were aligned relative to it.

3.2.2 Correspondence

Two different methods were tested to establish point-to-point correspondence: local feature similarity using Fast Point Feature Histograms and a custom heuristic henceforth referred to as Selective Sampling.

Fast Point Feature Histograms. (FPFH) are local descriptors which have been used in state-of-the-art applications for point cloud registration. This descriptor relies on the angular relationships between the normals of a given point and its neighbours to compute descriptive histograms. From these descriptors, correspondence can be established between points which have the most similar features by computing the histograms' distances (Rusu et al., 2009).

Selective Sampling: is based on a registration tech-



(a) Posterior view of TT socket. (b) Anterior-Medial view of TF socket.

Figure 2: Landmarks chosen for TT and TF sockets.

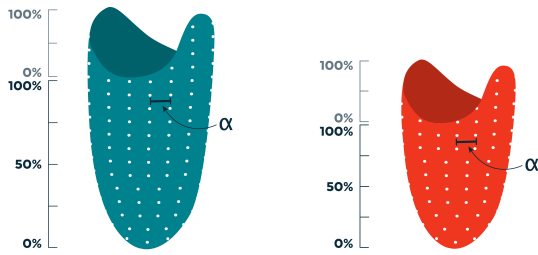


Figure 3: Two sockets registered through Selective Sampling. For a given height percentage h , a socket's circular profile has N points separated by an angle α .

nique often used in statistical shape models, which is parametrization by sampling evenly spaced points across a contour. Using domain knowledge and a more intuitive notion of correspondence, a similar approach which performs a selective sampling on the point clouds was designed. Two corresponding points can be thought of as points which are in the same relative position on two different sockets. Since the sockets are approximately paraboloids, this position can be defined by two values: the angle ω relative to a known vector and a percentage h of the height in two regions: above the landmark, and below the landmark. These two regions assure that the posterior and anterior support will always correspond across sockets, even if the lateral support's height differs between them.

The reference vector used to define the angle was the the origin-landmark vector OL used for alignment (where origin corresponds to the center of the circumference at the same z as the landmark). This vector is translated to a given height percentage h , OL_h and rotated around the z -axis in N intervals of α degrees. Rotating OL_h around the vertical z -axis by this angle creates a set P_i of evenly spaced target coordinates in the shape of a circular profile:

$$P_i(h, \omega) = OL_h \times R_z(i \times \alpha) \quad (1)$$

where $i \in [0, \dots, N]$ and R_z is the rotation matrix around z . Each point $P_i(h, \omega)$ in P_i is then matched to its closest neighbour in the point cloud A which has not yet been matched (to ensure a one-to-one correspondence):

$$P(h, \omega) = \arg \min_{p \in A} (\|p - P_i(h, \omega)\|) \quad (2)$$

The final registration result is then controlled by two parameters: N , the number of points in each circular profile, and K the number of profiles which should be sampled across the socket height. Figure 3 shows a schematic representation of the selective sampling process.

3.3 Model Building

With properly aligned and registered socket shapes, a statistical shape model F can be built from the dataset. PCA was performed for each separate type of socket, since the base designs of TT and TF vary considerably. To perform PCA on a registered training set, Singular Value Decomposition is applied to the shapes $F - \bar{F}$, where \bar{F} is the mean of the aligned shapes. The resulting matrix is a matrix P of eigenvectors, as well as their corresponding eigenvalues λ . Any valid shape set can then be defined as:

$$F = \bar{F} + \sum_{m=1}^M PC_m b_m \quad (3)$$

where M is the number of eigenvectors in the model (subspace dimension), b_m are scalar weights and PC_m are the principal components. To assure plausible variation, b_m has to be limited. Typical values to constrain this variation are $[-3\lambda_m, 3\lambda_m]$. For both TT and TF sockets, two different models were built, using the shapes registered through Selective Sampling and FPFH.

3.4 Evaluation

Generalization reflects the ability of a model to describe instances of the object that have not been seen during model building. If a model is overfitted, then its ability to generalize when faced with a new example will be very low. Generalization can be measured with a leave-one-out methodology (Davies et al., 2010).

Specificity is a measure of the similarity between generated shapes and the ones present in the training set. It is quantitatively defined by generating a new population of instances and averaging the distance between a new generated shape and the closest shape to it in the training set. The new population of instances should be created with weights that assure plausible shapes. This, combined with generalization, evaluates both the generative and reconstructive abilities of the model.

A visual expert evaluation was also performed by determining the individual meaning of each principal component (PC) captured by the model and attributing it an anatomical interpretation (when such interpretation existed in the prosthetics domain).

Generalization and specificity are two common approach-independent metrics used in the field (Davies et al., 2010). Due to the reduced size of the dataset, no explicit training/testing set division was done. This omission is counterweighted by the evaluation of generalization - a proxy metric of overfitting.

Table 2: Weight factors of each visually interpretable principal component, as validated by orthoprosthetists.

	PC1		PC2		PC3		PC4		PC5		PC6	
	Min	Max										
TT	-30	30	-	-	-20	30	-5	15	-	-	-15	15
TF	-30	30	-30	30	-15	10	-15	30	-12	12	-10	15

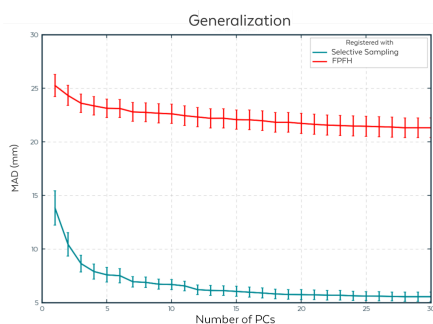


Figure 4: Generalization comparison between transtibial models registered through Selective Sampling and FPFH.

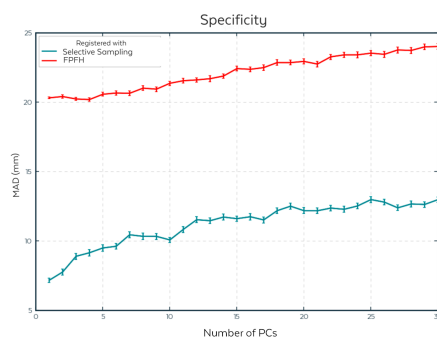


Figure 5: Specificity comparison between transtibial models registered through Selective Sampling and FPFH.

4 RESULTS

Results on generalization and specificity are presented for models based on point clouds registered through Selective Sampling and FPFH. This allows for a comparison between the accuracy of both methods, since a better registration will lead to a better model. Specificity and generalization were computed using as distance measure a normalized (by the number of points in question) Mean Absolute Distance (mean of the absolute distance between corresponding points, MAD).

Regarding expert evaluation, orthoprosthetists contributed to results by defining weight limits that assure the generation of plausible shapes (Table 2).

These weights were applied for the generation of new shapes, both for specificity calculation and for the visualization of PC effects on the average shape (using Equation (3)). For components with no visual interpretation, the weights used were $[-3\lambda_m, 3\lambda_m]$, as common in the literature.

Results subject to comparison were not found in the authors' literature review.

4.1 Transtibial Statistical Shape Model

4.1.1 Model Performance

By analysing the cumulative variance of the models, it is possible to determine how many PCs are required to obtain a descriptive model. To describe 95% of the variance in the training dataset, the Selective Sam-

pling model requires 6 PCs, while the FPFH one requires 22.

As shown in Figure 4, the model built from Selective Sampling registration has a lower reconstruction error, meaning better generalization. As expected, generalization improves with the number of principal components used for reconstruction. With 6 PCs, Selective Sampling produces a reconstruction error of 6.8 ± 1.8 mm, while FPFH at 22 PCs surpasses this error, with 21.6 ± 2.4 mm.

Specificity, which represents the similarity between the generated shapes and the ones present in the training set, is again superior using Selective Sampling (Figure 5), with an error of 9.7 ± 0.6 mm. Specificity is a crucial parameter in this work, given that one of the proposed applications is the creation of plausible shapes.

Since the models registered through Selective Sampling outperformed FPFH in all metrics, this model was chosen for the subsequent analyses.

4.1.2 Principal Component Analysis

In partnership with orthoprosthetists, it was possible to derive anatomical interpretations of the variance components captured by the model. PCs in which no relevant anatomical or design information was identified were omitted.

The first PC, which represents around 70% of the total variance, is related to the length of the residual limb, as can be seen in Figure 6. This is a natural variation, since the level of amputation is highly variable, depending on the patient's anatomy and injury degree.

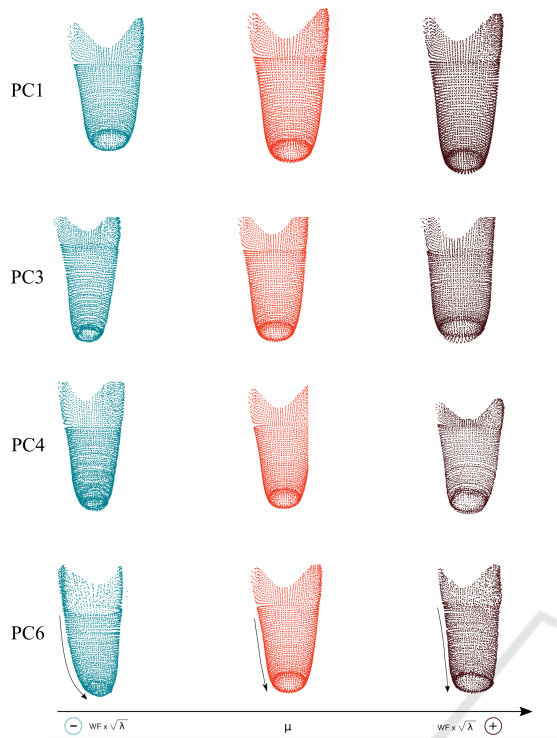


Figure 6: Representation of the principal components PC1 (residual limb length), PC3 (residual limb volume), PC4 (patellar coverage) and PC6 (medial leaning) with eigenvalues (λ), over the average transtibial shape (μ) and weight factors (WF) from Table 2 (posterior view).

The third PC, accounting for 5% of variance, corresponds to the circular profile variation along the longitudinal axis, distinguishing between more conical or cylindrical sockets. This is related to the musculature of the residual limb, which varies between subjects and also in time, since residual limbs are prone to atrophy and volume variations. Figure 6 shows this effect: the leftmost sockets exhibits perimeter reduction along its longitudinal axis, creating a conical shape, unlike the rightmost one, where the perimeter varies a lot less.

The fourth PC, responsible for 2.5% of the variance, is related to the level of coverage of the kneecap. Different designs can cover more or less of the knee structure, which is reflected in Figure 6. For instance, the leftmost socket, with higher lateral and medial walls and more patellar coverage, has a design evoking a suprapatellar patellar-tendon bearing socket (Paternò et al., 2018).

The sixth PC, representing 1% of the variance, represents a lateral-medial leaning in the socket (Figure 6), along with a narrowing of the distal end. This is frequently observed and depends on several factors: the level of amputation and the natural muscular profile and bone structure of the lower limb.

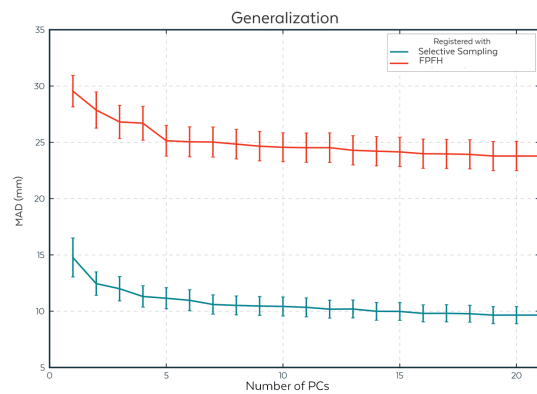


Figure 7: Generalization comparison between transfemoral models registered through Selective Sampling and FPFH.

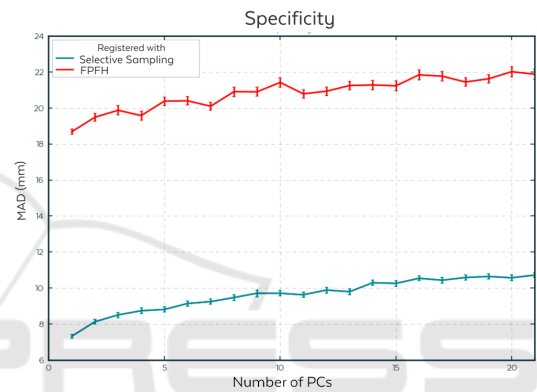


Figure 8: Specificity comparison between transfemoral models registered through Selective Sampling and FPFH.

4.2 Transfemoral Statistical Shape Model

4.2.1 Model Performance

A similar analysis to the one performed for the TT model can be done for the TF model. To describe 95% of the variance in the training dataset, the Selective Sampling model requires 11 PCs, while the FPFH one requires 16.

For a model with 11 PC, representing 95% of the variation in the training set, the generalization through Selective Sampling is 10.5 ± 1.6 mm, meaning an unseen shape would be, on average, reconstructed with this error. As shown in Figure 7, the Selective Sampling model again outperformed the FPFH registration. The generalization ability for this model is inferior to the one found for TT sockets.

Finally, the specificity of the TF model was also inferior to the TT one, with an error of 9.8 ± 0.2 mm for the Selective Sampling model (Figure 8).

Similarly to the TT case, the model registered

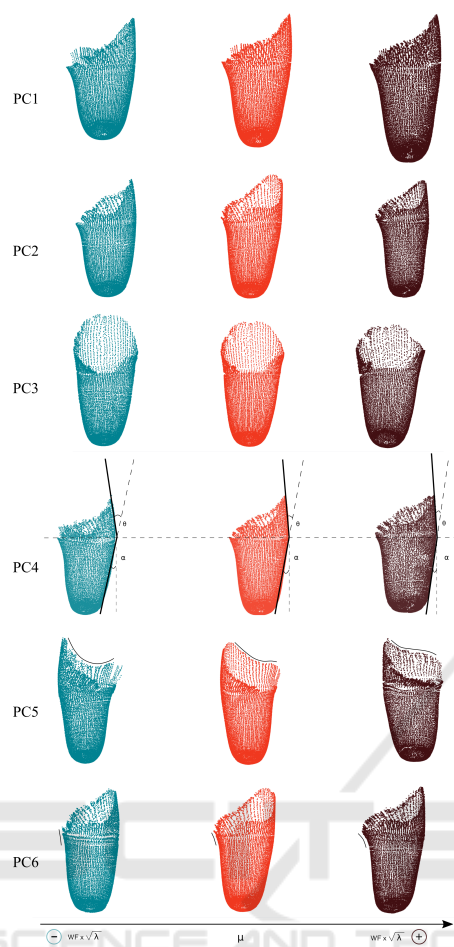


Figure 9: Representation of the influence of principal components: PC1 (residual limb length), PC2 (residual limb volume), PC3 (height of the lateral support), PC4 (adduction angle), PC5 (posterior proximal contour) and PC6 (ischial support) with eigenvalues (λ), over the average trans-femoral shape (μ), with weight factors (WF) from Table 2. PC1, PC2, PC4 and PC6 are shown in a posterior view, PC3 in a medial view and PC5 in an anterior view.

through Selective Sampling outperformed FPFH in all metrics, and was, therefore, the one chosen for subsequent analyses.

4.2.2 Principal Component Analysis

The most significant variation in the TF shapes is again relative to the length of the residual limb, representing 64% of the variance (Figure 9).

The second PC is related to the circular profiles along the longitudinal axis, responsible for 12% of variance. A more conical stump can be seen on the rightmost socket of Figure 9, while the leftmost one would be appropriate for a more cylindrical stump. This profile is dependent on the amputee's musculature and time after amputation, since the muscles are

subject to atrophy and volume reductions.

The third PC, which accounts for 5% of variance, represents the height of the lateral support. In Figure 9, the leftmost point cloud has a higher lateral support, which decreases in the shapes to its right.

PC number four is related with the adduction angle of the femur and the ilio-femoral angle, two important measurements taken during the fitting process, and represents 4% of variance. The first is defined between a longitudinal axis and the femur while in maximal adduction and is typically larger for women. The second is defined between the femur line and the lateral support. Figure 9 shows that, from left to right, these angles decrease.

The fifth PC varies the shape of the posterior proximal contour of the socket. In Figure 9, it is possible to see that the valley between the lateral and ischial support is more pronounced in the leftmost shape. This contour has an important effect in the aesthetic effect of the socket, as well as in comfort while sitting.

The sixth PC, which accounts for 2.5% of variance, is related to the prominence of the ischial seat. In Figure 9 (left of the top contour), it is possible to see that, from left to right, this support becomes wider and more pronounced.

5 DISCUSSION & CONCLUSIONS

By observing the features captured by the models, it is possible to conclude that they represent important anatomical variations in socket design - such as length and profile, in coherence with (Steer et al., 2020), but also subtler design characteristics. Given this, these models can be useful for generating new shapes with specific characteristics by manipulating the influence of their respective PCs. Additionally, the model's good generalization abilities allow it, for instance, to be used to reconstruct new 3D scans in socket acquisition systems, which may minimize acquisition artifacts.

The analysis performed showed the TT model outperformed the TF in all metrics. This can be due to a larger variation across base TF designs, which, in turn, can lead to a poorer registration process, or simply due to the lower number of samples used to build the model.

Two import aspects limit our work. Firstly, the high dependence on the registration process, which heavily impacts the input of the PCA model and, therefore, the accuracy of the results. To improve results and reduce that dependency, other more robust local descriptors could be tested. Secondly, the in-

ability to directly compare with other authors. This stems from the lack of relevant work in this field (as far as we were able to ascertain) and the lack of reference datasets for the task. Towards mitigating the latter, we are making some example data available in Section 6.

Nevertheless, this work shows that mathematically representing socket point cloud data through statistical shape models encodes biomechanically relevant information, allowing a range of potential applications with clinical interest like the generation of new plausible socket shapes (to support data-intensive learning workflows) or the automatic rotation of sockets' point clouds into relevant anatomical planes (for improved user experience in CAD/CAM software).

6 CONTRIBUTIONS

Some examples of TT and TF sockets shapes generated with the SSM are available on a GitHub repository: <https://github.com/adapttech-ltd/SocketSSM>.

REFERENCES

- Castellani, U. and Bartoli, A. (2014). 3D shape registration. In *3D Imaging, Analysis and Applications*, volume 9781447140, pages 221–264. Springer-Verlag London Ltd.
- Cha, J., Farhangi, M. M., Dunlap, N., and Amini, A. A. (2018). Segmentation and tracking of lung nodules via graph-cuts incorporating shape prior and motion from 4D CT. *Medical Physics*, 45(1):297–306.
- Cootes, T. F., Taylor, C. J., Cooper, D. H., and Graham, J. (1992). Active Shape Models-Their Training and Application. *Computer Vision and Image Understanding*, 61(1):38–59.
- Davies, R., Twining, C., Cootes, T., and Taylor, C. (2010). Building 3-D Statistical Shape Models by Direct Optimization. *IEEE Transactions on Medical Imaging*, 29(4):961–981.
- Huang, H., Brenner, C., and Sester, M. (2013). A generative statistical approach to automatic 3D building roof reconstruction from laser scanning data. *ISPRS Journal of Photogrammetry and Remote Sensing*, 79:29–43.
- Karakoç, M., Batmaz, I., Sariyildiz, M. A., Yazmalar, L., Aydin, A., and Em, S. (2017). Sockets Manufactured by CAD CAM Method Have Positive Effects on the Quality of Life of Patients With Transtibial Amputation. *American Journal of Physical Medicine & Rehabilitation*, 96(8):578–581.
- Lindner, C. (2017). Automated Image Interpretation Using Statistical Shape Models. In *Statistical Shape and Deformation Analysis: Methods, Implementation and Applications*, pages 3–32. Elsevier Inc.
- Mehmood, W., Abd Razak, N. A., Lau, M. S., Chung, T. Y., Gholizadeh, H., and Abu Osman, N. A. (2019). Comparative study of the circumferential and volumetric analysis between conventional casting and three-dimensional scanning methods for transtibial socket: A preliminary study. *Proceedings of the Institution of Mechanical Engineers, Part H: Journal of Engineering in Medicine*, 233(2):181–192.
- Paternò, L., Ibrahimi, M., Gruppioni, E., Menciassi, A., and Ricotti, L. (2018). Sockets for Limb Prostheses: A Review of Existing Technologies and Open Challenges. *IEEE Transactions on Biomedical Engineering*, 65(9):1996–2010.
- Pedregosa, F., Varoquaux, G., Gramfort, A., Michel, V., Thirion, B., Grisel, O., Blondel, M., Prettenhofer, P., Weiss, R., Dubourg, V., Vanderplas, J., Passos, A., Cournapeau, D., Brucher, M., Perrot, M., and Duchesnay, E. (2011). Scikit-learn: Machine learning in Python. *Journal of Machine Learning Research*, 12:2825–2830.
- Rusu, R. B., Blodow, N., and Beetz, M. (2009). Fast point feature histograms (fpfh) for 3d registration. In *2009 IEEE International Conference on Robotics and Automation*, pages 3212–3217.
- Steer, J. W., Worsley, P. R., Browne, M., and Dickinson, A. S. (2020). Predictive prosthetic socket design: part 1-population-based evaluation of transtibial prosthetic sockets by FEA-driven surrogate modelling. *Biomech Model Mechanobiol*, 19(4):1331–1346.
- Van Der Walt, S., Colbert, S. C., and Varoquaux, G. (2011). The numpy array: a structure for efficient numerical computation. *Computing in Science & Engineering*, 13(2):22.
- Varma, P., Stineman, M. G., and Dillingham, T. R. (2014). Epidemiology of limb loss. *Physical Medicine and Rehabilitation Clinics of North America*, 25(1):1–8.
- Wurdeman, S. R., Stevens, P. M., and Campbell, J. H. (2018). Mobility Analysis of Amputees II: Comorbidities and Mobility in Lower Limb Prosthesis Users. *American Journal of Physical Medicine and Rehabilitation*, 97(11):782–788.
- Yang, F., Metaxas, D., Wang, J., Shechtman, E., and Bourdev, L. (2011). Expression Flow for 3D-Aware Face Component Transfer. *ACM Transactions on Graphics*, 30(4):1–10.
- Yang, J., Cao, Z., and Zhang, Q. (2016). A fast and robust local descriptor for 3D point cloud registration. *Information Sciences*, 346-347:163–179.
- Zhou, Q.-Y., Park, J., and Koltun, V. (2018). Open3D: A modern library for 3D data processing. *arXiv:1801.09847*.